Available online at www.sciencedirect.com
ScienceDirect
Trans. Nonferrous Met. Soc. China 28(2018) 103−113
Transactions of Nonferrous Metals Society of China
www.tnmsc.cn

Physical and electromagnetic shielding properties of green carbon foam prepared from biomaterials

Shameel FARHAN[1], Ru-min WANG[1], Ke-zhi LI[2]

1. Department of Applied Chemistry, School of Science, Northwestern Polytechnical University, Xi'an 710072, China;
2. School of Materials Science and Engineering, Northwestern Polytechnical University, Xi'an 710072, China

Received 28 August 2016; accepted 6 November 2016

Abstract: 100% green carbon foam from the fibrous fruits of *Platanus Orientalis*-L (Plane) along with the tar oil as binder has been prepared using a powder molding technique. The objective was to develop a porous monolithic carbon from biomaterials with a considerable strength necessary for various physical, thermal and electromagnetic shielding applications. Fast carbonization was carried out at 1000 °C under the cover of Plane tree pyrolyzed seeds without using any external protective gas. For comparative analysis, some samples were mixed with 5% (mass fraction) iron chloride during the molding process. Iron chloride being a graphitization catalyst and activating agent helped in increasing the specific surface area from 88 to 294 m^2/g with a 25% decrease in flexural strength. Thermal stability was improved due to the incorporation of more graphitic phases in the sample resulting in a little higher thermal conductivity from 0.22 to 0.67 W/(m·K). The catalytic carbon foam exhibited shielding effectiveness of more than 20 dB over the X-band frequency. Absorption was dominant with only 8.26%−10.33% reflectance, indicating an absorption dominant shielding mechanism. The new material is quite suitable for high temperature thermal insulation being lightweight, highly porous with interconnected porous morphology most of which is preserved from the original biomaterial.
Key words: carbon foam; biomass; pyrolysis; powder molding; electromagnetic properties

1 Introduction

Carbon foams are inert materials with numerous applications in water and air purification technology, energy storage, radar absorbing materials, catalyst support, electrode materials, acoustic panel, tooling, and fuel cell humidification etc [1−3]. Most commonly, pitches, coals, and phenolic resin are used as carbonaceous precursors with self or induced foaming [4−6]. Due to importance of bio-based and environment-friendly precursors, tannin, cellulose, lignin and sucrose etc have also been utilized successfully for making such porous carbons [7,8]. Bio-based precursors can be agricultural residues, forestry products or city wastes and the resulting carbon is amorphous in nature. Recently, our research group has developed a novel powder molding method for making carbon foam [9,10]. Carbonaceous precursors containing pore former, binders, filler/additives (if any) in a required mixing ratio can be dry molded, cured and carbonized to make monolithic porous carbon with a desired morphology. In the current investigation, all bio-based carbon foam has been prepared by using powder molding method with carbonaceous precursors derived from non-food/non-feed plant origin. Woody fibrous powder and tar oil were used as pore former and binder, respectively. The Plane trees, the most common being *Platanus Orientalis* L (scientific name) or Wutong/Fatong (local Chinese name) is widely grown in the university campus and is one of the woody perennial trees of temperate regions [11]. The composition and vascular structure are responsible for the porosity development after thermal treatment in controlled environment [12]. Tar oil extracted from the woods becomes refractory after carbonization [13]. In addition, another goal of the current investigation was to produce bio-based carbon foam with a higher surface area using a graphitization catalyst during the carbonization processing. As reported earlier, chemical, physical, and a combination of physical/chemical

Foundation item: Project (CX201627) supported by the Innovation Foundation for Doctor Dissertation of Northwestern Polytechnical University, China
Corresponding author: Shameel FARHAN; Tel: +86-29-88492947; Fax: +86-29-88492943; E-mail: rmwang@nwpu.edu.cn, shameelfarhan@yahoo.com
DOI: 10.1016/S1003-6326(18)64643-6

processes are well-established methods for activation of carbonaceous materials [14−16]. Chemical activation process is simple and efficient as it takes place at a lower temperature with a shorter reaction time [17,18]. The most commonly used chemicals are zinc chloride ($ZnCl_2$), potassium hydroxide (KOH), phosphoric acid (H_3PO_4), sodium hydroxide (NaOH), iron chloride ($FeCl_3$) and phosphoric acid (H_3PO_4) etc [19,20]. For the current investigation, $FeCl_3$ was selected due to two reasons: first as a carbonization/graphitization d-metal catalyst and second as an activation agent [21]. One of the decisive factors, which determine the characteristic behavior of carbon foam, is the graphitization temperature. $FeCl_3$ played a major role in this regard by first dehydrating, then crosslinking and eventually promoting graphitization domains at carbonization temperature. Although many works have been published in recent years on the preparation of activated carbon from various cheaper and alternative agricultural wastes and by-products with chemical activation, there is no study about the preparation of "molded carbon foam" from 100% biomaterials and using $FeCl_3$ as activation/graphitization catalyst in one-step. Some works reported that tannin when being used for making bio-based carbon foam, presents tailor made and versatile properties but is low in density and not very high in strength [22]. Olive stones also resulted into carbon foam after pyrolysis under steam by the mechanism of softening and swelling but not in a bulk monolithic shape [23]. Therefore, the purpose of this work is to develop quasi-carbon foam with considerably high strength, bulk in shape, thermally insulating, shielding for electromagnetic interference (EMI) and extended surface properties. Carbon foams exhibit excellent EMI shielding as well as microwave absorption capacity, which could be closely ascribed to their tailored macrostructure, high electrical conductivity, good electromagnetism attenuation capability and highly porous interconnected framework [5,24,25]. Due to the synergetic effect of conductivity and multiple reflections, it is believed that this bio-based foam has promising shielding applications in harsh aircraft and other electronic enclosures.

2 Experimental

2.1 Preparation of precursors for carbon foam

Plane dried fruits were collected from the main university campus (Northwestern Polytechical University, Xi'an, China) and a part of it was used to make tar oil. Starch and $FeCl_3.6H_2O$ were purchased from Sino-pharm Chemical Reagent Beijing Co., Ltd. The dried fruits were washed with a liquid soap and dried at 110 °C for 24 h. After crushing, grinding and sieving using a 50-mesh screen, the proximate analysis of Plane fruit powder (PFP) showed 12.94% of moisture, 58.48% of volatile matter, 13.84% of ash, 14.74% of fixed carbon. The high contents of organic compounds (74.99%) indicate that it has a potential as a good carbon precursor. Tar oil was made by devolatilization of hard Plane fruit seeds in an enclosed reactor (Fig. 1) in a temperature range of 400−500 °C. The heat was supplied from the outer source and the pyrolysis reaction was started from the bottom side being close to the heat source. Most of the heat was consumed by the endothermic pyrolysis reaction at the wall sides. By this time, the solids at the top of the reactor and away from heat source were heated very slowly and most of carbon was converted into the char. The pyrolytic vapors from the bottom initiated secondary cracking reaction at the top producing more yield of char in this reactor.

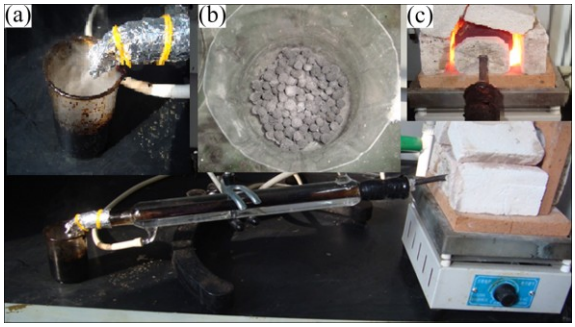

Fig. 1 Tar extraction set-up: (a) Tar oil collection; (b) Carbonized seeds; (c) Heating furnace with heating from one (bottom) side

The non-condensing gases (CO_2, CO, CH_4, H_2, H_2O, and C_xH_y) were escaped and a liquid tar was collected in a beaker. Due to the presence of aldehydes and low molecular-mass acids, the tar oil had a strong smoky odor — a characteristic of liquids obtained by the pyrolysis process. Visual characteristics of the as-prepared char and tar oil are shown in Fig. 1; the physical properties are presented in Table 1. The yield of tar oil and char was calculated based on mass ratios (total yield in mass/total precursor mass × 100%). In this lab scale process, carbonized seeds and tar oil were produced

Table 1 Physical properties of tar oil and char

Sample	Density/(g·cm^{-3})	Yield/%	Water content (mass fraction)/%	Viscosity/(mPa·s)	pH
Tar oil	1.07[a]	35−39	11−15[c]	3.12	3.3−3.5
Char	0.035[b]	25−29	–	–	–

a: Density measurement bottle; b: Density of one seed; c: Karl Fischer titrimetric method

simultaneously in one step, yielding about 27% and 37%, respectively.

2.2 Preparation of green foam

The PFP and starch were mixed at a ratio of 9:1 by mass. $FeCl_3$ being hygroscopic was mixed with tar oil at a ratio of 9.5:0.5. Finally, both the reagents were mixed together at 1:1 ratio by mass so that $FeCl_3$ was 5% (mass fraction) of the PFP and hence the resulting green carbon foam was hereafter abbreviated as GCFe5. In another kind of recipe, no $FeCl_3$ was mixed in the tar oil and hence the obtained green carbon foam was called GCFe0. The mixed dough was stabilized at room temperature for 24 h. After ensuring a good homogeneity, calculated amount of dough was filled in a rectangular mold and pressed tightly. The amount of mixture in the mold determines the final density of the carbon foam; the greater the quantity is, the higher the final density will be. The molded mixture was cured after a thermal cycle of 120 °C for 2 h followed by 140 °C for 2 h, 160 °C for 2 h and finally 180 °C for another 2 h. The cured foam shrank consistently while preserving the initial shape and remained monolithic. Figure 2 shows various stages of material preparation and molding for making carbon foam.

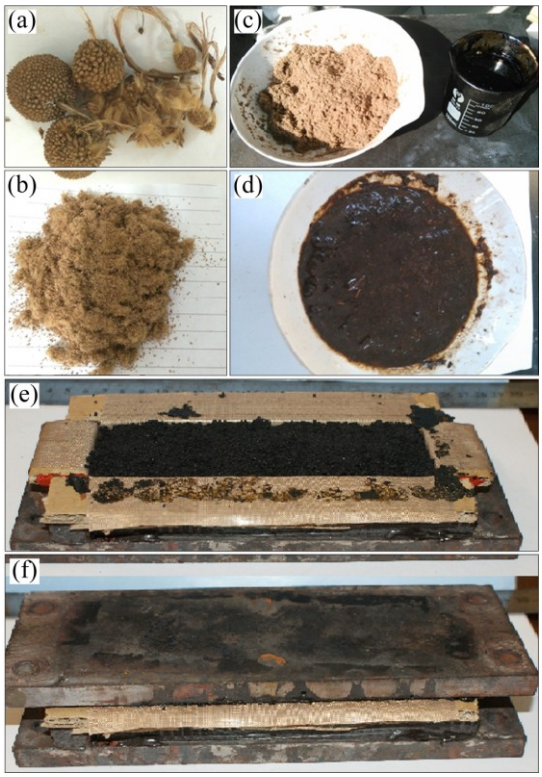

Fig. 2 Material preparation for carbon foam: (a, b) Plane tree fruits and powder; (c) PFP and tar oil; (d) Mixed dough for room temperature stabilization; (e) Mold filling with stabilized semi-solid dough; (f) Molding closing

2.3 Carbonization of green foam

High temperature treatment of green foam was carried out in a steel container filled with the carbonized seeds produced during tar oil formation (Fig. 1(a)). A small nozzle was fitted at the top, which was connected with an exhaust pipe for the removal of gases generated during pyrolysis. The container was placed in an oven and heated up to 1000 °C (oven temperature was set to be 1150 °C) at the rate of 200 °C/h and after reaching the target temperature, the samples were kept in the operating furnace for 8 h. After 8 h, the furnace was switched off, and the carbonization container was allowed to cool down to room temperature thereafter. After pyrolysis treatment, the carbon foams were weighed and measured dimensionally to record the mass losses and volume shrinkages during the processing, respectively. The obtained carbon foam was repeatedly washed with 0.2 mol/L solution of HCl, to remove the metallic components. Figure 3 shows the schematic of carbonization container and removal of excess iron after pyrolysis treatment.

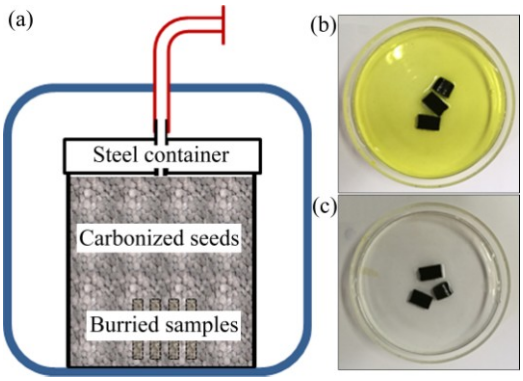

Fig. 3 Carbonization of carbon foam: (a) Schematic representation of carbonization container; (b) Washing in 0.2 mol/L HCl; (c) Neutralized samples

2.4 Characterization of carbon foams

The apparent bulk density (ρ_a) was calculated from the physical dimensions and mass of rectangular specimens. A helium gas displacement pycnometer (Pentapyc 5200e Quantachrome Instruments, Florida, USA) was used for the calculation of true density and apparent porosity. The true density (or skeletal density, ρ_t) is the mass of carbon skeleton divided by its volume excluding open and closed pores and voids. Before measurements, the specimens were crushed in an agate mortar and pestle, degassed in a vacuum oven at 120 °C overnight, and stored in sealed envelopes. Equation (1) was used to calculate the bulk porosity (p) as follows:

$$p = \left(\frac{\rho_t - \rho_a}{\rho_t} \right) \times 100\% \quad (1)$$

The thermal behavior was measured with a thermo gravimetric analyzer (Shimadzu, TG/DTA−50). About 10 mg of sample was heated from 25 to 1000 °C at a rate of 10 °C/min under oxygen atmosphere, and constantly weighed. Phase analysis was carried out in an X-ray diffractometer (XRD) (Philips analytical PW 1710) using Cu K_α radiation of 1.5418 Å at 40 kV and 30 mA. Three-point bending tests were conducted on an electronic universal testing machine (SANS CMT 4304, Shenzhen, China) using some guidelines from ASTM C−1341. The test parameters used were as follows: sample dimensions of 90.0 mm × 12.0 mm × 6.0 mm, crosshead speed of 0.5 mm/min and loading span of 60 mm. Flexural strength was calculated using

$$\sigma = \frac{3PL}{2bh^2} \tag{2}$$

where P is the force (N) at fracture point, L is the length (mm) of the supported span, b is the width (mm) and h is the thickness (mm).

The thermal diffusivity of carbon foam samples was determined at 25 °C using a Netzsch LFA 457 laser flash apparatus. The thermal diffusivity was measured on samples with dimensions of d12.5 mm × 3.0 mm (ASTM E 1461). The thermal conductivity of at least three specimens was determined. The sample density ρ_a and specific heat capacity C (measured using the differential scanning calorimeter, Netzsch STA 449C) were used to calculate the thermal conductivity:

$$\lambda = \rho a C \tag{3}$$

where λ is thermal conductivity (W/(m·K)), ρ is the density (kg/m^3), a is thermal diffusivity (m^2/s) and C is specific heat capacity (J/(kg·K)).

The general morphology was examined using a JEOL JSM−6490LV scanning electron microscope (SEM) with an operating voltage of 20 kV. Nitrogen adsorption and desorption isotherms were performed at −196 °C on a Micromeritics ASAP 2010 volumetric adsorption system for the evaluation of textural properties using a wide range of pressure. The isotherms were measured over a relative pressure (equilibrium pressure/saturation pressure of the adsorbate at −196 °C, P/P_0) range of approximately 10^{-6} to 1.0. Total surface area and pore volumes were determined using the Brunauer–Emmett–Teller (BET) equation and the single point method, respectively. The adsorption branch of nitrogen isotherm was used to calculate pore size distribution (PSD) using the density functional theory [26]. Bulk electrical conductivity of specimens with dimension of 22.86 mm × 10.16 mm × 4.00 mm was measured by four probe method using a current source (Keithley 6221 DC, Ohio, USA) and a nano-voltmeter (Model 2182A). The EMI shielding properties were measured using a waveguide method with a two-port vector network analyzer (VNA; MS4644A, Anritsu, Kana-gawa, Japan). The specimens used for measuring electrical conductivity were fixed in the cavity and scanned in X band (8.2−12.4 GHz). The total shielding effectiveness (E_T), absorption shielding effectiveness (E_A) and reflection shielding effectiveness (E_R) were calculated by Nicolson-Ross and Weir–NRW algorithm using scattering parameters.

3 Results and discussion

3.1 Physical and thermal properties of carbon foam

Table 2 gives the density, porosity and surface properties of GCFe0 and GCFe5 green carbon foams. Bulk density depends on the quantity of stabilized dough filled in the mold. For current investigation, it came out to be 0.54 and 0.58 g/cm^3 for GCFe0 and GCFe5, respectively. During high temperature treatment, carbon foam mostly rearranged into structures of more aromatic character through thermal annealing process. The mass losses after carbonization were somewhat lower than those reported in Ref. [27].

The GCFe0 and GCFe5 exhibited thermal conductivities of (0.22±0.02) and (0.67±0.02) W/(m·K), respectively. The lower thermal conductivity of GCFe0 was due to random and non-graphitizing structure, which conducts heat much less effectively than the aligned graphitic planes. This result is remarkable for a material with such a low density (0.58 g/cm^3) suitable for thermal insulation especially for high temperature applications in inert atmosphere. For GCFe5, its thermal conductivity increased to 0.67 W/(m·K) that is about two times higher than that of GCFe0 but still not very high to be used for applications requiring high thermal conductivity. Pores in the carbon foam contributed substantial effect on the overall thermal conductivity and hence a higher porosity posed a negative effect on the rise as was expected due to higher graphitic domains in GCFe5 green carbon foam. TGA is a very useful technique for analyzing the purity and the thermal oxidation properties of carbon materials [28]. Graphitized carbons with a higher degree

Table 2 Physical, structural and textural properties of GCFe0 and GCFe5

Sample	Density/ (g·cm^{-3})	Mass loss/%	Volume shrinkage/%	Porosity/ %	Thermal conductivity/ (W·m^{-1}·K^{-1})	S_{BET}/ (m^2·g^{-1})	Micro pore volume/ (cm^3·g^{-1})	Total pore volume/ (cm^3·g^{-1})
GCFe0	0.58	62−64	57−59	68.02	0.22±0.02	88	0.05	0.52
GCFe5	0.54	64−65	54−56	74.79	0.67±0.02	294	0.16	0.63

of graphitization are more stable against oxidation than amorphous carbons. The difference between amorphous and graphitic carbons can be found to some extent when the samples are slowly oxidized in TGA mode. The resulting curves of thermal analyses of GCFe0 and GCFe5 are shown in Fig. 4.

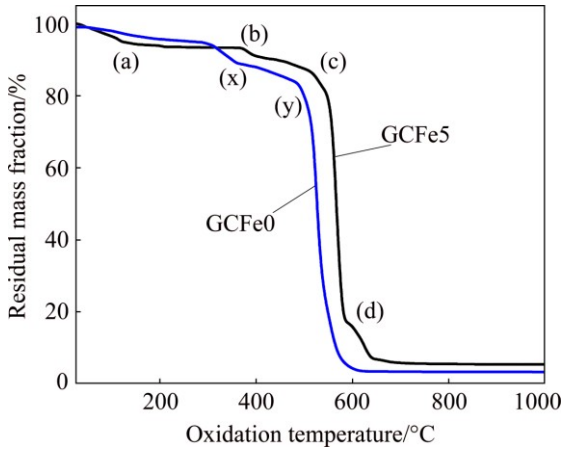

Fig. 4 TGA curves of GCFe0 and GCFe5 carbon foams heated in oxygen atmosphere

The GCFe5 shows four distinctive steps of mass losses indicating that the sample is composed of multiple forms of carbon (amorphous and crystalline): Step (a) around 110 °C due to evaluation of moisture/vapors, Step (b) around 390 °C due to reaction of more amorphous and more reactive carbon, Step (c) around 530 °C due to reaction of bulk graphitic carbon and Step (d) around 580 °C due to layer by layer oxidation. Step (a) is also indicative of development of more surface area in GCFe5 as compared to that of GCFe0. The GCFe0 also exhibited the similar behavior but merely in two steps: at (x) around 350 °C similar to that of Step (b) and at (y) similar to that of Step (c). The graphitic stages in GCFe5 are better graphitized than those in GCFe0. It can be concluded that the prepared GCFe5 carbonaceous material consists of an amorphous and graphitic carbon and combusts in a multi-stage process over a broader temperature range with a higher thermal stability [29].

3.2 Phase and microstructure analysis of carbon foam

To further explore the phases and crystallinity, XRD analysis was carried out, as shown in Fig. 5. The (002) band is generally accepted as the average stack height of the aromatic planes of carbon crystallite, while the (004) reflections at 61°−62° are characteristics of 2D and 3D graphitic structures [27]. Two broad peaks, (002) and (100), appearing around approximately at 25° and 43°, respectively, represent the formation of hexagonal graphitic structures. XRD pattern of the GCFe5 carbon foam revealed diffraction peaks at 44.7° and 83° due to the presence of α-Fe metallic particles although the sample was acid washed after carbonization. Asymmetry of the diffraction peaks shows that there is always a mixture of graphite and amorphous carbon [30]. In the GCFe0 carbon foam, the diffractions of graphitic carbon were superimposed by broad amorphous carbon reflections and hence became very unclear. In the GCFe5 carbon foam, (002) peak became sharper, narrower and shifted slightly towards that expected of graphite, indicating an increase in the degree of graphitization. This was due to the presence of $FeCl_3$ as catalyst during pyrolysis treatment and peaks at 26°, 43°, 54° and even at 78° are assigned to the (002), (100/101), (004) and (110) diffractions of the graphitic structure, respectively.

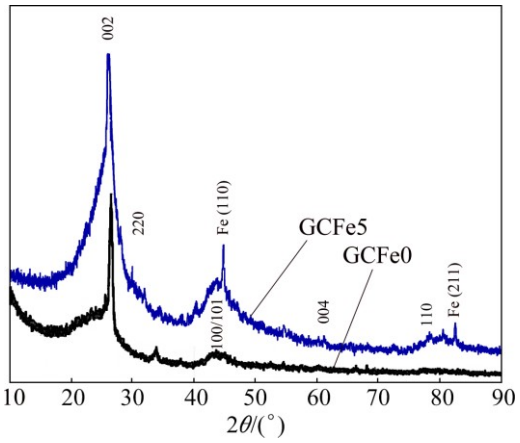

Fig. 5 XRD spectra of GCFe0 and GCFe5 carbon foams

During pyrolysis treatment, some of the Fe nanoparticles sintered together forming larger and immobilized particles. Consequently, the carbon located far from the metallic nanoparticles retained its amorphous structure. Therefore, interpenetrating amorphous and graphitic carbon domains were obtained. Figure 6 shows a hierarchical quasi-foam structure of the GCFe0 and GCFe5 carbon foams. The images of the GCFe5 showed some cavities caused by chemical activation with $FeCl_3$ during carbonization. $FeCl_3$ catalyzed the polymerization reactions commonly designated as Scholl condensation reactions between tar-forming compounds and aromatic hydrocarbons in the structure of precursor. These also result in the formation of larger polycyclic aromatics in the structure of carbon foam and increase the carbon yield. The Scholl condensation reactions by the reaction with Lewis acids, is known to be very efficient for the cyclode-hydrogenation of aromatic compounds. The resulting polycyclic compounds moved away from the structure during the heat treatment leaving behind a porous body. Both the carbon foams possess a compact, biomorphic and anisotropic porous structure built up of interconnected flakes with disordered voids. Overall, the morphology showed a rougher texture with

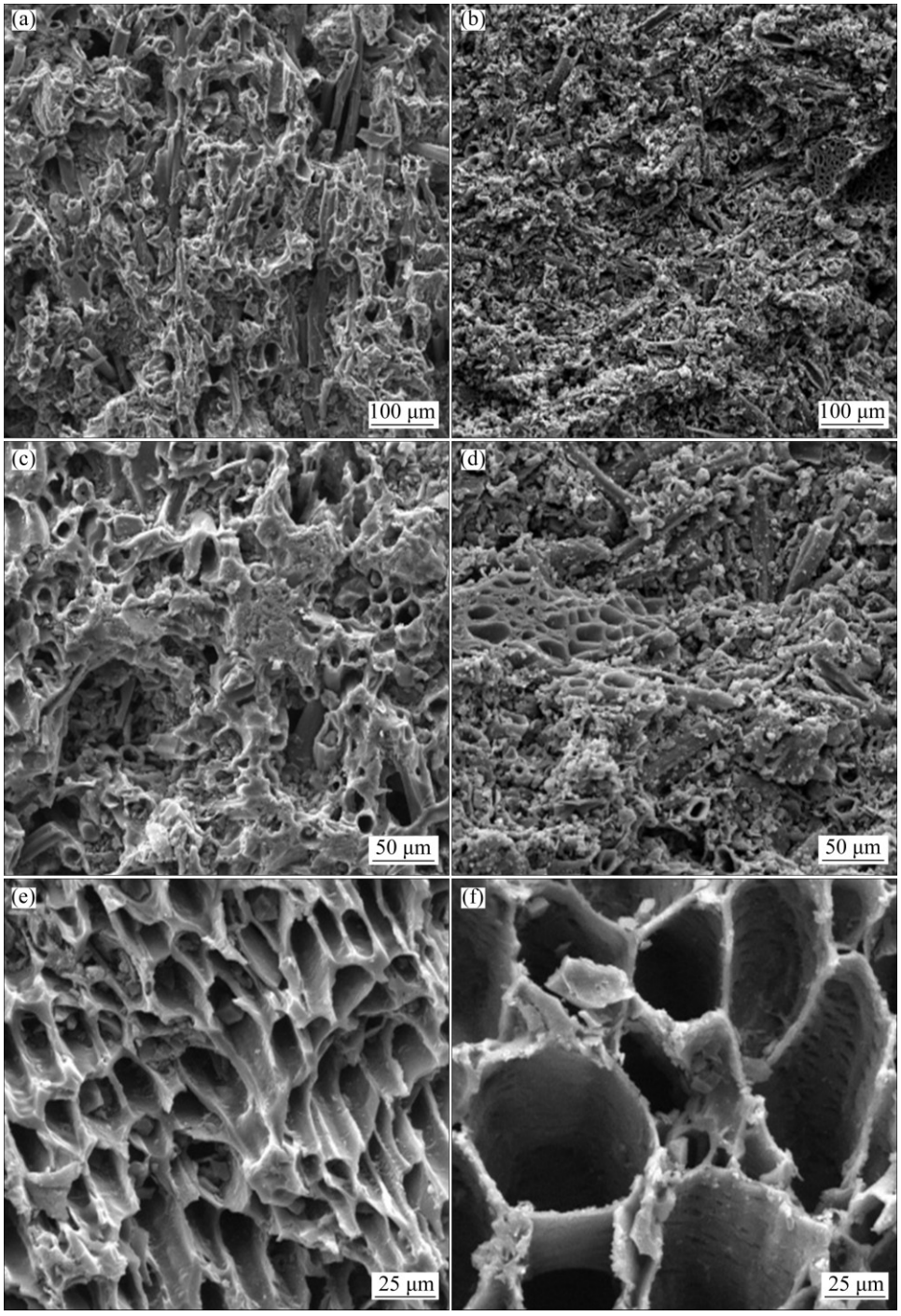

Fig. 6 SEM micrographs: (a, c, e) GCFe0; (b, d, f) GCFe5

heterogeneous surfaces and a greater variety of randomly distributed pore sizes ranging up to 50 μm. Channels of different shapes were inherited from the structures of Plane fruit seeds. The residual structure of cells and directional patterns of fibrils in the PFP were also preserved. Activation resulted in the creation of more pores, with some micropores created by gasification, as shown in Fig. 6(f). As listed in Table 2, the porous properties of GCFe5 in this work are superior to those of GCFe0. It can be ascertained that a carbon foam with a BET specific surface area ≥ 294 m^2/g could be produced with other more commonly used activating agents like $ZnCl_2$ and KOH. In other words, the solid grinding with mold curing and carbonization can be a useful approach to produce monolithic carbon foams with a high surface area.

3.3 Mechanical properties and surface area analysis

Figure 7 exhibits the isotherm of the GCFe0 and GCFe5 carbon foams resembling a type IV and type II

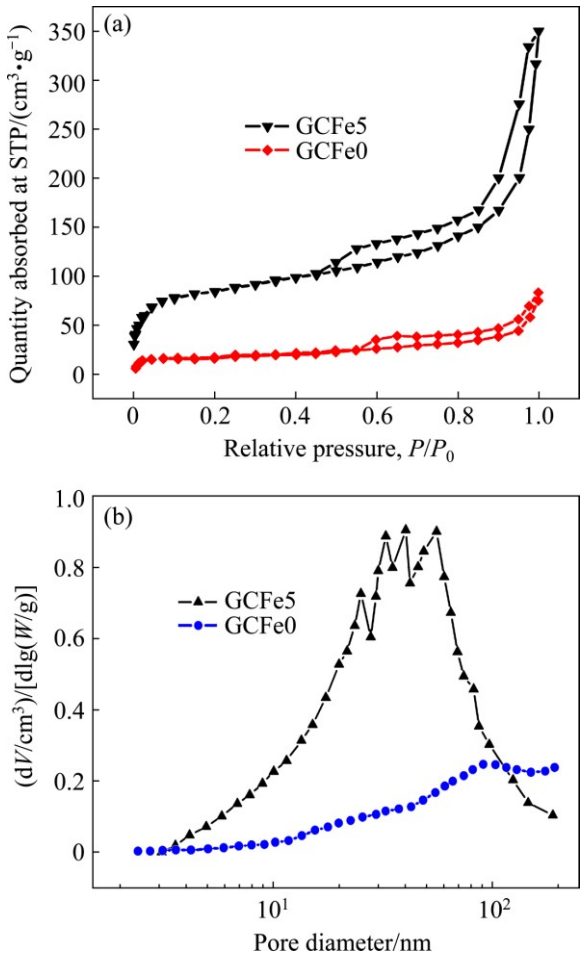

Fig. 7 N_2 adsorption isotherm (a) and pore size distribution (b) of GCFe0 and GCFe5 carbon foams

IUPAC (International Union of Pure and Applied Chemistry) isotherms with H3 or H4 hysteresis loop, respectively [31]. The loops are located between the relative pressure of 0.45 and 1.0. The hysteresis loop is the characteristic feature of the type IV isotherm, which is due to capillary condensation inside the mesopores and limiting uptake over a high range of relative pressure. This is indicative of the presence of constrictions in the porous network and also evident in SEM images. The GCFe5 showed a BET surface area of 294 m^2/g and a pore volume of 0.60 cm^3/g, which is associated to framework-confined mesopores. The type II isotherm is usually obtained with a macro porous materials representing unrestricted adsorption [32]. Type H3 loop with unlimited adsorption at a high relative pressure is generally observed for materials with plate-like particles and slit-shaped pores whereas the H4 loop is often associated with narrow slit-like pores. In this case, the N_2 isotherms above relative pressure of 0.95 did not reach saturation, confirming that the carbon foams are macro porous materials with some mesoporosity. For GCFe5, four well-distinguished regions with relative pressure are evident: (1) micropore volume filling at 0.05, (2) monolayer-multilayer adsorption at 0.25, (3) capillary condensation at 0.45 and (4) multilayer adsorption on the outer surfaces of particles at 0.99. The GCFe5 possesses well-developed micro porosity as compared to that of GCFe0 carbon foam showing a reduced micro porosity. A steep rise of N_2 adsorption at relative pressure lower than 0.01 is always associated with the existence of micro pores which are almost absent in case of GCFe0 carbon foam. In situ activation due to the formation of CO during carbonization under the cover of carbonized seeds is responsible for the micro pore generation in the GCFe5 carbon foam. Furthermore, from the pore size distribution curves shown in Fig. 7(b), it can be seen that the pores with the diameter >10 nm contribute to most of the total pore volume being centered at 30−60 nm. The GCFe0 showed a very shallow distribution curve with majority of pores in diameter >100 nm. The GCFe5 shows a reasonably high specific surface area but still superior and can be further improved by additional activation step. This novel hierarchical structure is believed to provide a potential platform for designing new materials.

For mechanical characterization of prepared carbon foam, flexural testing was carried out due to two reasons: one due to mold size being long and thin and second unidirectional compaction in the mold making carbon foam two dimensional in nature. The load–displacement curves (not shown here) indicate a brittle behavior for all the samples including those carbonized with $FeCl_3$. The curves were almost linear up to the maximum load with an ultimate strength in the range of 9–12 MPa. The mechanical performance of GCFe5 was greatly affected by higher surface area and porosity, showing a lower modulus and brittle fracture. Higher strength and more zigzag fracture in CFFe0 before ultimate failure was due to short fur like fibrils that acted as a barrier against fracture to some extent by fiber pulling-out, debonding and crack deflection. It can be noticed that no appreciable difference is observed for these samples, despite the different levels of porosity and mechanical properties of the carbonized fibrils. SEM analysis of the fracture surfaces revealed fiber debonding and delamination although these fibers are not as strong as other reinforcing fibers like carbon, glass and SiC. The values of flexural strength are not easily found in the literature, and hence, the specific strength being 17−20 $MPa·cm^3/g$ was reasonable for high temperature structural elements.

3.4 EMI shielding effectiveness

During high-temperature heat-treatment of carbonaceous material with $FeCl_3$, some oxides of Fe are formed which then undergo carbo-thermal reduction to elemental Fe. Along with these reactions, graphitic

structure is also developed and the yield depends on the concentration of Fe particles, pore structure and carbonization temperature [33]. In the current work, 5% (mass fraction) catalyst was used which was actually even lower if compared to total amount of carbon precursors (PFP, tar and starch). The purpose of this preliminary work is to develop representative green carbon foam, which can be further analyzed using various concentrations of $FeCl_3$. During carbonization, following in situ reactions also known as dissolution–precipitation reactions occur [34]:

$$Fe+Amorphous\ C \longrightarrow Fe_3C \quad (4)$$

$$Fe_3C \longrightarrow Fe+Graphitic\ C \quad (5)$$

Being an excellent graphitization catalyst, Fe particles were produced during pyrolytic pore development in carbon foam [35,36]. Since the $FeCl_3$ was mixed well in the dough and the resulting Fe particles too into the porous carbon, the difference in the adhesive forces between $C_{amorphous}$–Fe and $C_{graphite}$–Fe was the driving force for the graphite formation. The electrical conductivity of green carbon foam was calculated based on the following equation:

$$R=\frac{l}{\sigma \cdot A} \quad (6)$$

where l is the length, σ is the electrical conductivity, and A is the cross-sectional area.

In a single-phase porous body, electrical conductivity increases linearly with the increase of relative density due to the decrease in current path flow [37]. The GCFe0 showed a lower conductivity of 3.31×10^{-1} S/m, which was due to the ribbon like graphite structure, formed by the carbonization of biomass. The GCFe5 displayed a relatively higher conductivity of 1.18×10^{3} S/m, which was increased roughly by four orders of magnitude, compared to that of the GCFe0 carbon foam. Electrical conductivity depends on the graphitization degree and a significant increase was due to the formation of locally interconnected graphitic nanostructures. For most of dielectric materials, the relative permittivity (ε_r), a characteristic of dielectric properties, is mainly affected by conductivity loss, as represented by the imaginary part (ε'') [38,39]. As shown in Fig. 8, the complex permittivity decreased non-linearly with increasing frequency in the X band. It was due to the reduction of electric field induced in the porous body in response to the reversing external electric field by the delay in molecular polarization. This phenomenon is known as dielectric relaxation, and it reflects the irreversible degradation of free energy [40]. Permittivity and permeability are intrinsic properties but the absorptivity may depend on polarization of incoming wave [41]. As compared to GCFe5, the complex permittivity for GCFe0 was small (11.50−i7.47) and decreased slightly in the X-band. Dielectric loss tangent ($\tan\delta=\varepsilon''/\varepsilon'$) was calculated to clarify the incident EM wave attenuation. As shown in Fig. 8(c), the $\tan\delta$ was higher, being in the range of 1.1−1.0 for GCFe5, which is better for EM wave attenuation and could be concluded from the Debye dipolar relaxation [41]. Presence of Fe particles during carbonization created very small graphitic domains resulting in an increase in the number

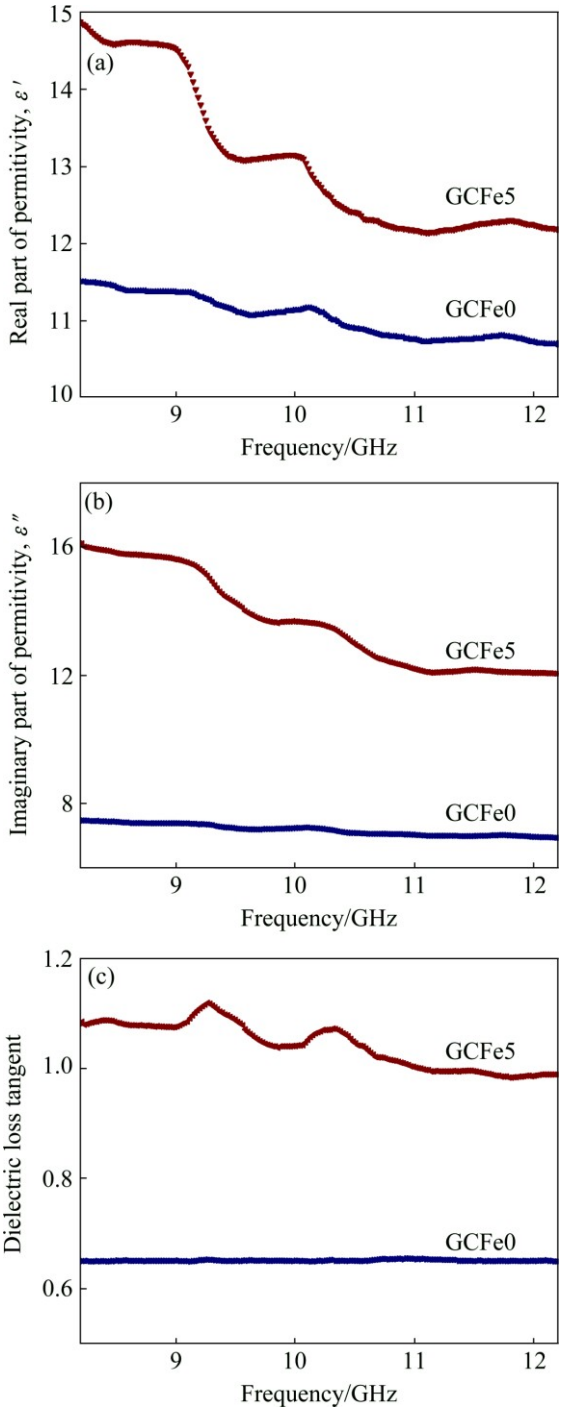

Fig. 8 Relative complex permittivity and loss tangent of GCFe0 and GCFe5 green carbon foams: (a) Real part of permittivity; (b) Imaginary part of permittivity; (c) Dielectric loss tangent

of surface atoms with unsaturated bonds. This phenomenon caused an increase of the dipoles. These conductive micro-network structures with multi-interfaces made the micro-current exhausted in the foam, resulting in a strong conductive loss and increased EM attenuation. As shown in Fig. 8, the maximum ε' and ε'' values came out to be 14.88 and 16.10, respectively. All these parameters along with tan δ were strongly affected by the creation of graphitic domains in foam. EMI shielding effectiveness for a shield is described as follows [42,43]:

$$E_T=E_R+E_A+E_M \quad (7)$$

$$E_R\approx-10\times\lg(1-R) \quad (8)$$

$$E_A\approx-10\times\lg(T/(1-R)) \quad (9)$$

$$E_T\approx E_A+E_R=10\times\lg(P_{in}/P_{out}) \quad (10)$$

The reflection (R) and transmission (T) coefficients can be calculated according to following equations [44]:

$$T=|S_{12}|^2=|S_{21}|^2=P_{out}/P_{in} \quad (11)$$

$$A=1-R-T \quad (12)$$

$$R=|S_{11}|^2=|S_{22}|^2=P_{ref}/P_{in} \quad (13)$$

As shown in Fig. 9, the E_T value of GCFe5 was always above 20 dB over the whole range, which was due to the generated graphitic networks offering mobile charge carriers to move and interact with the EM field [45]. Moreover, due to higher values of E_A, absorption dominant EMI shielding mechanism seemed to be dominant. In porous materials, the polarization loss can be regarded as an integrated factor arising from pores and interfaces [39]. In porous bodies, the EM waves suffer multi-scattering and multi-reflection on the pore walls as soon as they enter into the pores larger than the wavelength of EM wave [46].

In this work, the intra-pores and inter-pores, as shown in Fig. 2, are less than 200 μm, whereas the wavelength of the EM waves in X-band is 2.50−3.75 cm. Under this circumstance, the losses of incident EM waves in carbon foam were simply caused by the dissipation of electric current in the pore walls. In the case of GCFe5, the imaginary part was slightly higher than that of the real part which is beneficial for high absorption [47]. The specific shielding effectiveness (E_{ST}, EMI shielding effectiveness/density) of the GCFe5 came out to be 40 dB·cm^3/g which is four times that of solid copper. In the case of GCFe5, the graphitic structure and a higher electrical conductivity played an important role in shielding effectiveness. The graphitic structure decreased the effective permittivity and increased the absorption losses, resulting in an overall increase of shielding effectiveness.

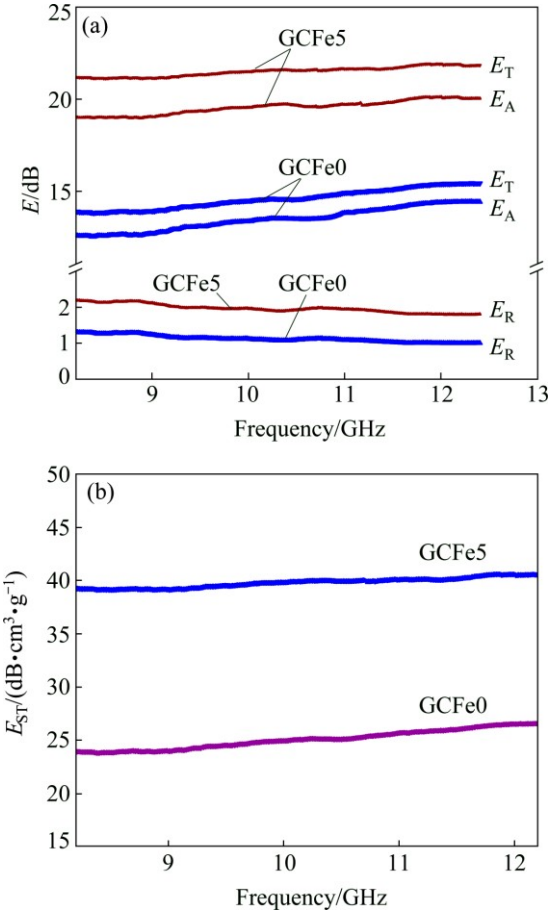

Fig. 9 Electromagnetic shielding effectiveness of GCFe0 and GCFe5 carbon foam samples: (a) E_T, E_A and E_R; (b) E_{ST} in X band

4 Conclusions

100% bio-based carbon foam was prepared using a powder molding method. The obtained carbon foams presented a high porosity, excellent thermal insulation and appropriate microwave absorption. In situ activation, catalytic graphitic domains at carbonization temperature and all bio precursors have the characteristic features of monolithic carbon foam. The resulting carbon foam possesses well-developed macro, meso and micro porosity where from an application perspective the macro porosity is also very important for low flow-through mass transfer resistance. This novel hierarchical structure is believed to provide a platform for designing new materials indicating its advantages as a kind of structural and functional materials for EMI shielding applications.

References

[1] FARHAN S, WANG Ru-min. Thermal, mechanical and self-destruction properties of aluminum reinforced carbon foam [J]. Journal of Porous Materials, 2015, 22: 897−906.

[2] SONG Yun-feng, WANG Xian-you, BAI Yan-song, WANG Hao, HU Ben-an, SHU Hong-bo, YANG Xiu-kang, YI Lan-hua, JU Bo-wei, ZHANG Xiao-yan. Preparation and performance of hierarchically porous carbons as oxygen electrodes for lithium oxygen batteries [J]. Transactions of Nonferrous Metals Society of China, 2013, 23(12): 3685−3690.

[3] WOJNICKI M, PACŁAWSKI K, SOCHA R P, FITZNER K. Adsorption and reduction of platinum(IV) chloride complex ions on activated carbon [J]. Transactions of Nonferrous Metals Society of China, 2013, 23(4): 1147−1156.

[4] CHEN C, KENNEL E B, STILLER A H, STANSBERRY P G, ZONDLO J W. Carbon foam derived from various precursors [J]. Carbon, 2006, 44(8): 1535−1543.

[5] FARHAN S, WANG Ru-min, LI Ke-zhi. Carbon foam decorated with silver particles and in situ grown nanowires for effective electromagnetic interference shielding [J]. Journal of Materials Science, 2016, 51: 7991−8004.

[6] FARHAN S, WANG Ru-min, JIANG Hao, UL-HAQ N. Preparation and characterization of carbon foam derived from pitch and phenolic resin using a soft templating method [J]. Journal of Analytical and Applied Pyrolysis, 2014, 110: 229−234.

[7] PIZZI A, TONDI G, PASCH H, CELZARD A. MALDI-TOF structure determination of complex thermoset networks–Polyflavonoid tannin–furanic rigid foams [J]. Journal of Applied Polymer Science, 2008, 110: 1451−1456.

[8] TONDI G, PIZZI A. Tannin-based rigid foams: Characterization and modification [J]. Industrial Crops and Products, 2009, 29: 356−363.

[9] FARHAN S, WANG Ru-min, JIANG Hao. A novel method for the processing of carbon foam containing in situ grown nano-materials and silicon nanowires [J]. Materials Letters, 2015, 159: 439−442.

[10] FARHAN S, WANG Ru-min, JIANG Hao, LI Ke-zhi. Use of waste rigid polyurethane for making carbon foam with fireproofing and anti-ablation properties [J]. Materials and Design, 2016, 101: 332−339.

[11] TANTRY M A, AKBAR S, DAR J A, IRTIZA S, MOHAMMAD A G, KHUROO M A, GHAZANFAR K. Acylated flavonol glycoside from Platanus orientalis [J]. Fitoterapia, 2012, 83: 281−285.

[12] VALENTE NABAIS J, LAGINHAS C, RIBEIRO CARROTT M M L, CARROTT P J M, CRESPO AMOROS J E, NADAL GISBERT A V. Surface and porous characterization of activated carbons made from a novel biomass precursor, the esparto grass [J]. Applied Surface Science, 2013, 265: 919−924.

[13] GOSSELINK R J A, KEOSSE A M A, van der PUTTEN J C, van der KOLK J C, de KLERK ENGELS B, van DAM J E G, Wood preservation by low-temperature carbonization [J]. Industrial Crops and Products, 2004, 19: 3−12.

[14] SEJIRIFA M L, MAHAMMED M H, PALLIER S, BAAMEUR L, RICHARD D, AL DUJAILI A H. Preparation and characterization of an activated carbon from a date stones variety by physical activation with carbon dioxide [J]. Journal of Analytical and Applied Pyrolysis, 2013, 99: 155−160.

[15] MATOS J, LABADY M, ALBORNOZ A, LAINE J, BRITO L. Topological organization and textural changes of carbon macro-networks submitted to activation with N_2 and CO_2 [J]. Journal of Materials Science, 2004, 39: 3705−3716.

[16] GONZALEZ J F, ROMAN S, ENCINAR J M, MARTINEZ G, Pyrolysis of various biomass residues and char utilization for the production of activated carbons [J]. Journal of Analytical and Applied Pyrolysis, 2009, 85: 134−141.

[17] YORGUN S, VURAL N, DEMIEAL H. Preparation of high-surface area activated carbons from Paulownia wood by $ZnCl_2$ activation [J]. Microporous and Mesoporous Materials, 2009, 122: 189−194.

[18] ZUBIZARRETA L, ARENILLAS A, PIS J J, PIRARD J P, JOB N. Studying chemical activation in carbon [J]. Journal of Materials Science, 2009, 44: 6583−6590.

[19] EL HENDAWY A A. Surface and adsorptive properties of carbons prepared from biomass [J]. Applied Surface Science, 2005, 252: 287−295.

[20] MACIA J A, MOORE B C, CAZOELA AMOROS D, LINARES SOLANO A. Activation of coal tar pitch carbon fibres: Physical activation vs. chemical activation [J]. Carbon, 2004, 42: 1367−1370.

[21] SEVILLA M. Catalytic graphitization of templated mesoporous carbons [J]. Carbon, 2006, 44(3): 468−474.

[22] TONDI G, FIERRO V, PIZZI A, CELZARD A. Tannin-based carbon foam [J]. Carbon, 2009, 47: 1480−1492.

[23] RIOS R V R A, ESCANDELL M M, SABIO M M, REINOSO F R. Carbon foam prepared by pyrolysis of olive stones under steam [J]. Carbon, 2006, 44(8): 1448−1454.

[24] MOGLIE F, MICHELI D, LAURENZI S, MARCHETTI, MARIANI PRIMIANI V. Electromagnetic shielding performance of carbon foams [J]. Carbon, 2012, 50(5): 1972−1980.

[25] FARHAN S, WANG Ru-min, LI Ke-zhi. Electromagnetic interference shielding effectiveness of carbon foam containing in situ grown silicon carbide nanowires [J]. Ceramics International, 2016, 42: 11330−11340.

[26] JAGIELLO J, THOMMES M. Comparison of DFT characterization methods based on N_2, Ar, CO_2, and H_2 adsorption applied to carbons with various pore size distributions [J]. Carbon, 2004, 42: 1227−1232.

[27] EL SHEIKH A H, NEWMAN A P, AL DAGGAEE H K, PHULL S, CRESSWELL N. Characterization of activated carbon prepared from a single cultivar of Jordania olive stone by-chemical physicochemical techniques [J]. Journal of Analytical and Applied Pyrolysis, 2003, 71: 151−164.

[28] XIA Lun-gang, ZHANG Hong-bo, XIONG Xiang. Effects of heat treatment temperature on oxidation behavior of glass-like carbon derived from acetone-furfural resin [J]. Transactions of Nonferrous Metals Society of China, 2011, 21(2): 330−334.

[29] ZHANG Yong, TANG Yuan-hong, LIN Liang-wu, ZHANG En-lei. Microstructure transformation of carbon nanofibers during graphitization [J]. Transactions of Nonferrous Metals Society of China, 2008, 18(8): 1094−1099.

[30] ZHANG Wu-zhuang, ZENG Yi. Preparation and oxidation property of ZrB_2−$MoSi_2$/SiC coating on carbon/carbon composites [J]. Transactions of Nonferrous Metals Society of China, 2011, 21(7): 1538−1544.

[31] SAKA C. BET, TG–DTG, FT-IR, SEM, iodine number analysis and preparation of activated carbon from acorn shell by chemical activation with $ZnCl_2$ [J]. Journal of Analytical and Applied Pyrolysis, 2012, 95: 134−141.

[32] ROUQUEROL F, ROUQUEROL J, SING K. Adsorption by powders and porous solids: Principles, methodology and applications [M]. London: Academic Press, 1999.

[33] SEVILLA M, SALINAS MARTINEZE DE LECEA C, VALDES SOLIS T, MORALLON E, FUERTES A B. Solid-phase synthesis of graphitic carbon nanostructures from iron and cobalt gluconates and their utilization as electrocatalyst supports [J]. Physical Chemistry and Chemical Physics, 2008, 10: 1443−1452.

[34] HARRIS P J F. New perspectives on the structure of graphitic carbons [J]. Critical Review in Solid State Materials Science, 2005, 30: 235−253.

[35] ZHOU Hai-hui, PENG Qi-ling, HUANG Zhen-hua, YU Qiang, CHEN Jin-hua, KUANG Ya-fei. Catalytic graphitization of PAN-based carbon fibers with electrodeposited Ni−Fe alloy [J]. Transactions of Nonferrous Metals Society of China, 2011, 21(3): 581−587.

[36] ZHOU Shao-yun, LI Xin-hai, WANG Zhi-xing, GUO Hua-jun, PENG Wen-jie. Effect of activated carbon and electrolyte on

properties of supercapacitor [J]. Transactions of Nonferrous Metals Society of China, 2007, 17(6): 1328−1333.

[37] JIA Yan, LI Ke-zhi, XUE Li-zhen, REN Jun-jie, ZHANG Shou-yang, LI He-jun. Mechanical and electromagnetic shielding performance of carbon fiber reinforced multilayered (PyC-SiC)*n* matrix composites [J]. Carbon, 2017, 111: 299−308.

[38] SING A P, MISHRA M, CHANDRA A, DHAWAN S K. Graphene oxide/ferrofluid/cement composites for electromagnetic interference shielding application [J]. Nanotechnology, 2011, 22(46): 465701−465704.

[39] MICHELI D, MORLES R B, MARCHETTI M, MOGLIE F, MARIANI PRIMIANI V. Broadband electromagnetic characterization of carbon foam to metal contact [J]. Carbon, 2014, 68: 149−158.

[40] WANG Chao, HAN Xi-jiang, XU Ping, ZHANG Xiao-lin, DU Yun-chen, HU Su-rong, WANG Jing-yu, WANG Xiao-hong. The electromagnetic property of chemically reduced graphene oxide and its application as microwave absorbing material [J]. Applied Physics Letters, 2011, 98(7): 072906−072909.

[41] GRADONI G, MICHELI D, MOGLIE F, MARIANI PRIMIANI V. Absorbing cross section in reverberation chamber: Experimental and numerical results [J]. Progress in Electromagnetics Research B, 2012, 45: 187−202.

[42] MA Yu-zhao, YIN Xiao-wei, LI Quan. Effects of heat treatment temperature on microstructure and electromagnetic properties of ordered mesoporous carbon [J]. Transactions of Nonferrous Metals Society of China, 2013, 23(6): 1652−1660.

[43] YIN Xiao-wei, XUE Ye-ye, ZHANG Li-tong, CHENG Lai-fei, Dielectric, electromagnetic absorption and interference shielding properties of porous yttria-stabilized zirconia/silicon carbide composites [J]. Ceramics International, 2012, 38(3): 2421−2427.

[44] AL SALEH M H, SUNDARARAJ U. X-band EMI shielding mechanisms and shielding effectiveness of high structure carbon black/polypropylene composites [J]. Journal of Physics D: Applied Physics, 2013, 46: 035304−035310.

[45] LIU Qing-lei, ZHANG Di, FAN Tong-xiang, GU Jia-jun, MIYAMOTO Yo-shinari, CHEN Zhi-xin. Amorphous carbon-matrix composites with interconnected carbon nano-ribbon networks for electromagnetic interference shielding [J]. Carbon, 2008, 46(3): 461−465.

[46] YIN Xiao-wei, KONG Luo, ZHANG Li-tong, CHENG Lai-fei, TRAVITZKY N, GREIL P. Electromagnetic properties of Si−C−N based ceramics and composites [J]. International Materials Reviews, 2014, 59(6): 326−355.

[47] HUYNEN I, QUIEVY N, BAILLY C, BOLLEN P, DETREMBLEUR C, EGGERMONT S, MOLENBERG I, THOMASSIN J M, URBANCZYK L, PARDEON T. Multifunctional hybrids for electromagnetic absorption [J]. Acta Materilia, 2011, 59: 3255−3266.

由生物材料制备的绿色碳泡沫的物理及电磁屏蔽性能

Shameel FARHAN[1]，王汝敏[1]，李克智[2]

1. 西北工业大学 理学院 应用化学系，西安 710072；
2. 西北工业大学 材料学院，西安 710072

摘　要：以梧桐树含纤维的果实为原料、煤焦油沥青为粘合剂，通过粉末模塑法制备了 100%绿色碳泡沫，目的是采用生物材料制备高强度，且可应用于物理、热和电磁屏蔽领域的多孔碳泡沫。在 1000 °C 下不使用任何外部保护性气体，通过对梧桐树种子热解进行快速碳化。为比较分析，模制过程中在一些样品中混入了 5%(质量分数)的氯化铁。氯化铁作为石墨化催化剂和活化剂，使材料比表面积从 88 增加到 294 m^2/g，弯曲强度降低 25%。由于材料中引入较多的石墨成分，其热稳定性得到改善，但热导率提高有限(从 0.22 提高到 0.67 W/(m·K))。经催化得到的碳泡沫在 X 波段的电磁屏蔽效能在 20 dB 以上，反射率仅为 8.26%~10.33%，表明吸收损耗是占主导地位的电磁屏蔽机理。这种新材料轻质、高度多孔，保留有机生物材料互连多孔形态，有望应用于高温隔热材料领域。

关键词：碳泡沫；生物质；热解；粉末模塑；电磁特性

(Edited by Bing YANG)